Journal of Power Sources 214 (2012) 51–58

Contents lists available at SciVerse ScienceDirect

Journal of Power Sources

journal homepage: www.elsevier.com/locate/jpowsour

The characteristics and performance of electroless nickel and immersion Au plated aluminum alloy bipolar plates in polymer electrolyte membrane fuel cells

Sung-Ying Tsai [a], Ching-Yuan Bai [b], Chien-Hung Lin [c], Gia-Nan Shi [a], Kung-Hsu Hou [d], Yih-Ming Liu [b], Ming-Der Ger [b,*]

[a] School of Defense science, Chung Cheng Institute of Technology, National Defense University, Tao-Yuan 335, Taiwan, ROC
[b] Electrochemical Microfabrication Lab, Department of Chemical and Materials Engineering, Chung Cheng Institute of Technology, National Defense University, Tau-Yuan 335, Taiwan, ROC
[c] Department of Physics, R.O.C Military Academy, Kaohsiung 830, Taiwan, ROC
[d] Department of Power Vehicles and System Engineering, Chung Cheng Institute of Technology, National Defense University, Tao-Yuan 335, Taiwan, ROC

HIGHLIGHTS

► Au/Ni–P multilayer coatings on Al-alloy BPPs.
► Using electroless nickel immersion gold technique to prepare complex coatings.
► Al-alloy BPP with Au/Ni–P coating has excellent conductivity and corrosion resistance.

ARTICLE INFO

Article history:
Received 26 February 2012
Received in revised form
15 April 2012
Accepted 16 April 2012
Available online 28 April 2012

Keywords:
Electroless nickel
Immersion gold
Aluminum alloy bipolar plates
Interfacial contact resistance
Electrochemical impedance
Power density

ABSTRACT

Cheap, lightweight, and malleable Al-alloy 5052 is suggested as alternative materials of graphite bipolar plates (BPPs) in proton exchange membrane fuel cells (PEMFCs). This work presents the first research in producing Au/Ni–P multilayer coatings on Al-alloy BPPs using an electroless Ni–P along with immersion gold techniques. The modified Al-alloy BPPs are investigated to evaluate the coating structure, corrosion resistance, interfacial contact resistance, electrochemical impedance of single cells, and single cell performance. The results indicate that the Al-alloy BPPs with Au/Ni–P coatings, in which Ni–P is prepared at pH 4.5, reveal the lowest contact resistance and the best corrosion resistance ($I_{corr} = 8.43 \times 10^{-6}$ A cm^{-2}) in a 0.5 M H_2SO_4 + 2 ppm HF solution among all of the modified specimens. The electrochemical impedance of the Au/Ni–P coating after long-term operation is 9.1 mΩ. In addition, the power density of the single cells assembled with the Au/Ni–P/Al-alloy BPPs is 0.84 W cm^{-2} measured at a cell voltage of 0.7 V, comparable to that with graphite BPPs (0.80 W cm^{-2}), in the test conditions of this study. We find that the Au/Ni–P multilayer coating is very appropriate for modifying Al-ally BPPs in PEMFC systems.

1. Introduction

The proton exchange membrane fuel cell (PEMFC) is one of the most valuable fuel cell systems. It possesses the advantages of working at low temperature, starting quickly, and converting hydrogen and oxygen (or air) to electricity with water as the only residual product [1,2]. The bipolar plate (BPP) is one of the significant parts of the cell stack in PEMFC systems [2,3]. Conventionally, substrates made of graphite have been generally used as bipolar plates in PEMFCs. However, the bipolar plates make up about eighty percent of the fuel cell stack's mass and volume, impeding fuel cells from the commercial feasibility [4]. The employment of metallic BPPs has received attention recently due to the ease of manufacturing a flow-field pattern and the consideration in designs of a smaller and thinner stack. However, the inferior corrosion resistance of metals and the high contact electrical resistance induced by the formation of oxide on the metal surface, unfortunately, would result in poisoning the membrane [5,6] and deteriorate the performance of fuel cells [6,7]. Therefore, suitable coatings must be employed to improve surface characters of the metal bipolar plate.

In general, Al alloys have the characteristics of lightweight, high specific strength and rigidity, inexpensive price, and easy processing [5]. The cheap and malleable aluminum alloy 5052 is

* Corresponding author. Tel.: +886 3 3891716; fax: +886 3 3892494.
E-mail address: mingderger@gmail.com (M.-D. Ger).

0378-7753/$ – see front matter © 2012 Elsevier B.V. All rights reserved.
doi:10.1016/j.jpowsour.2012.04.030

therefore suggested as alternative materials of graphite plates in this research to lower the manufacturing cost of BPPs and allow the designs of smaller and thinner stacks in PEMFCs. However, surface modification of the Al-alloy bipolar plate must be done to achieve the anti-corrosion and high conductivity properties [8]. Lin et al. performed a research on anti-corrosion properties and structures of Ni–P coatings produced via an electroless method. The results showed that the Ni–P coating prepared at pH 4.3 and 70 °C possessed an amorphous structure and the best corrosion resistance ($I_{corr} = 3 \times 10^{-5}$ A cm^{-2}) [9]. Moreover, Bai et al. carried out an investigation on anti-corrosion properties of Al bipolar plates with Ni–Mo–P deposits. The deposit produced in the electrolyte with 4.13×10^{-2} M Na_2MoO_4 at pH 7.0 and 70 °C showed the lowest corrosion density ($I_{corr} = 4 \times 10^{-6}$ A cm^{-2}). Nevertheless, a few metal ions were still dissolved from the bipolar plates for a long-term test period [10]. It is obvious that the Ni-based alloy coating can improve anti-corrosion property of Al alloys, but the improving efficiency of Ni-based alloys is insufficient for using in PEMFC environment.

So far, noble metals with excellent chemical nobility and electrical conductivity are regarded as the protector of metal bipolar plates [11,12]. This is the most mature and effective surface modification technique to improve metal BPPs, but the price of noble metals is expensive. Therefore, how to enhance the effect and reduce the consumption of noble metals becomes the key technology. Wang et al. electroplated a gold coating with thickness of about 2 μm on a titanium bipolar plate. The results showed that after surface modification the single cell performance was better than the graphite bipolar plates [13]. Jung et al. also deposited gold coatings on titanium plates by sputtering method. The results showed that when the thickness of gold coating was less than 0.8 μm, the cell performance decreased rapidly during cycling test because of the coating deterioration. According to the previous reports mentioned above, the feasibility of improving the performance of metal bipolar plates via gold coatings was proved [14]. Moreover, it is necessary to enhance the denseness and reduce the defects of gold coatings in order to reduce the gold usage.

For resolving the problems faced in metal bipolar plates and the preparation of precious metal plating, this study presents the first research in producing complex coatings using an electroless Ni–P along with immersion gold techniques. The electroless Ni–P coatings were firstly produced on the Al bipolar plate at various pH values to increase its corrosion resistance [15–17]. Next, electroless nickel immersion gold (ENIG) technique was used to prepare gold coatings on the Ni–P alloys. The ENIG method can produce a dense and low porosity gold coating, which is difficult to prepare by electroplating gold technique [18,19], and therefore the thickness of gold coating for protecting metal bipolar plates can be less than 1 μm. In this work, the relationship between coating conditions and operating parameters of electroless Ni–P and immersion gold processes is examined. Moreover, the structure and composition of the electroless Ni–P alloys were modulated to produce a quality gold coating with high conductivity and excellent corrosion resistance. Finally, the performance of single cell assembled with surface modified bipolar plates was investigated and discussed.

2. Experimental

2.1. Fabrication of metal bipolar plates

Al-alloy 5052 with surface roughness (R_a) of about 0.28 μm was used as the substrate material of bipolar plates. The chemical composition of Al-alloy 5052 is listed in Table 1. The surface morphology of machined substrates was not modified in order to increase the contact area of the BPP and gas diffusion layer (GDL), because the contact resistance between BPP and GDL can be effectively diminished by texturing the surface morphology of BPP to match the morphology of GDL.

Table 1
The chemical composition of aluminum alloy 5052 (in wt%).

Elements	Si	Fe	Cu	Mg	Ti	Mn	Cr	Zn	Al
wt%	0.25	0.4	0.10	2.8	0.15	0.1	0.15	0.1	Rest

The aluminum substrate was pre-treated for Zn replacement in two steps prior to the Ni–P electroless deposition process. The bath composition and deposition conditions of Zn replacement are listed in Table 2. Step one – The specimens were immersed in a NaOH base solution (pH 12) for 3 min, and cleaned with deionized water. A nitric acid solution (30% HNO_3) was used to pickle the surface of the specimens for 3 min, and the specimens were cleaned with deionized water again. The surface replacement of Zn was then practiced by dipping the specimens in the Zn electrolyte for one min. Step two – The specimens that underwent the step one were immersed in a nitric acid solution (30% HNO_3) for 2 min, and cleaned with deionized water. Then, the specimens were dipped in the Zn electrolyte for 2 min. After two steps of the Zn replacement procedure, the specimens were immersed into a Ni–P electroless solution at various pH values and 85 °C to produce the Ni–P deposits on the substrates. The depositing bath and conditions for preparing Ni–P coatings are listed in Table 3. Following the Ni–P deposition procedures, the specimens with Ni–P deposits were conducted the immersion Au process. The depositing bath and conditions for preparing immersion Au coatings are listed in Table 4. The Ni–P coatings prepared at pH 4.5, 5.5, and 6.5, were denoted as NDU-EN-1, NDU-EN-2, and NDU-EN-3, respectively. The corresponding specimens subjected to the immersion Au process were, accordingly, denoted as NDU-ENIG-1, NDU-ENIG-2, and NDU-ENIG-3.

2.2. Materials analyses and electrochemical test

Surface morphologies, cross-sectional microstructures, and chemical compositions of the deposits were examined by field emission scanning electron microscopy (FE-SEM) with X-ray energy dispersive spectrometry (EDS), and electron probe micro-analysis (EPMA) with X-ray wavelength dispersive spectrometry (WDS). The crystal structures of Ni–P deposits were characterized using a grazing incidence (incident angle of 0.5°) X-ray diffractometer with monochromatic Cu-Kα radiation generated at 25 kV and 25 mA (wavelength = 1.542 Å).

The potentiodynamic polarization was employed to investigate the general corrosion behaviors of the Ni–P and Au coatings exposed area of about 1 cm^2 in a 0.5 M H_2SO_4 + 2 ppm HF solution without purging any gases at room temperature. A standard three-electrode cell system with Ag/AgCl (197 mV versus SHE), platinum electrode, and the specimens were used as a reference, counter, and working electrode, respectively. The specimens were initially stabilized in the solution at open circuit for 3 min, and then the scan was started from this open circuit potential. The sweeping potential

Table 2
The bath composition and operating conditions of Zn replacement.

Bath composition and parameters	Concentration/Condition
NaOH	12.5 M
ZnO	0.92 M
$FeCl_3.6H_2O$	0.0037 M
$NaNO_3$	0.012 M
$KNaC_4H_4O_6.4H_2O$	0.0071 M
Bath temperature	25 °C

Table 3
Bath composition and deposition conditions for Ni–P plating.

Bath composition and parameters	Concentration/Condition
$NiSO_4.6H_2O$	0.11 M
$C_3H_5O_3Na$	0.08 M
$NaH_2PO_2.H_2O$	0.28 M
$C_2H_5O_2N$	0.13 M
Bath temperature	85 °C
Deposition time	30 min
Solution pH	4.5, 5.5, 6.5

range was from −0.25 V to +0.25 V referred to the open circuit potential with a scanning rate of 0.166 mV s^{-1}.

2.3. Interfacial contact resistance (ICR) measurement

In this work, the interfacial contact resistance between the specimen and gas diffusion layer was evaluated with the measurement techniques well documented in our previous reports [20]. Fig. 1 shows the schematic diagram of the measurement method for interfacial contact resistance between the coated Al-alloy BPPs and GDLs, which is similar to the report found by Wang et al. [21]. The range of the operating load was 0–196 N cm^{-2} for recording ICR values at every 9.8 N cm^{-2}. The total resistance of combined components shown in Fig. 1 can be measured depending on the compaction force, and the ICR values can be derived by Eq. (1).

$$\mathrm{ICR} = \frac{R - R_{cp}}{2} \times A \quad (1)$$

where R, R_{cp}, and A are on behalf of measured total resistance, resistance of carbon paper (GDL), and surface area, respectively. Besides, the resistance of carbon paper used in this work is about 3.8–7.2 mΩ.

2.4. Single cell tests

The bipolar plate used in this work was machined a single serpentine flow-field pattern with an area of 25 cm^2 (5 cm × 5 cm), as shown in Fig. 2. Single PEM cells were fabricated with the Ni–P or Au/Ni–P coated Al-alloy BPPs. The membrane electrode assembly (MEA) consisted of Nafion-112 membranes and Torry paper with a catalyst loading of 0.2 mg cm^{-2} on anode and 0.4 mg cm^{-2} on cathode electrode. The active area of the Nafion-112 membrane was 25 cm^2.

Prior to the cell operation, nitrogen was used to purge the cell of residual gases. Pure hydrogen and oxygen were used as reactant gases at the anode and cathode sides with the flow rates of 210 sccm and 140 sccm, respectively. The temperature of the fully humidified flow gas and cell was set at 333 K. Cell voltages as a function of current density for the tested single cells were measured in the operation region of 0.9–0.35 V. Moreover, initial and long-term electrochemical impedance spectroscopy (EIS) measurements of single cells were conducted in the testing

Table 4
Bath composition and deposition conditions for Au immersion plating.

Bath composition and parameters	Concentration/Condition
$KAu(CN)_2$	0.03 M
NH_4Cl	0.72 M
$C_6H_5Na_3O_7.2H_2O$	0.20 M
Bath temperature	90 °C
Deposition time	15 min
Solution pH	7.0

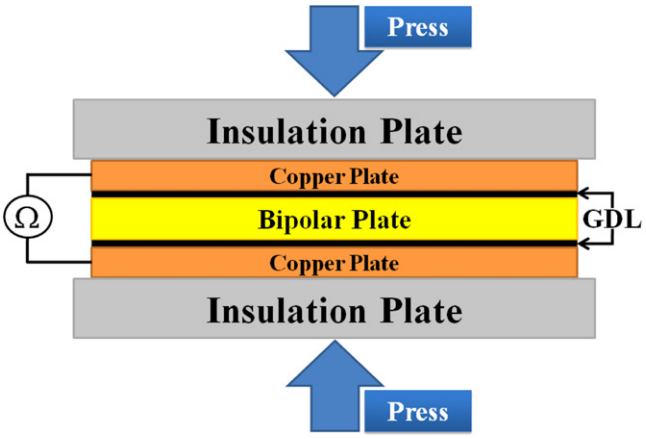

Fig. 1. The schematic diagram of interfacial contact resistance test.

environment of 0.6 V and 333 K. Each EIS spectrum was recorded to construct the Nyquist plots. In the impedance spectroscopy spectra of Nyquist plots, the high frequency intercept of the single impedance arc on the real axis (R_Ω) represents the total ohmic resistance of the cell. The cell ohmic resistance can be expressed as the sum of the contributions from contact resistances between components and ohmic resistances of the cell components such as the membrane, catalyst layer, gas diffusion layer, and bipolar plates. Moreover, the diameter of the kinetic loop, R_{ct}, is a measure of the charge transfer resistance of the oxygen reduction reaction [23]. Then, the impedance spectra can be used to determine the cell resistance and evaluate the decay factors of cell performance.

3. Results and discussion

3.1. Effect of bath pH on the structure of N–P coatings

High contact resistance existing in the interface between BPPs and GDLs is one of the most important issues of metallic bipolar plates. The contact resistance between BPP and GDL can be effectively diminished by modifying the surface composition and

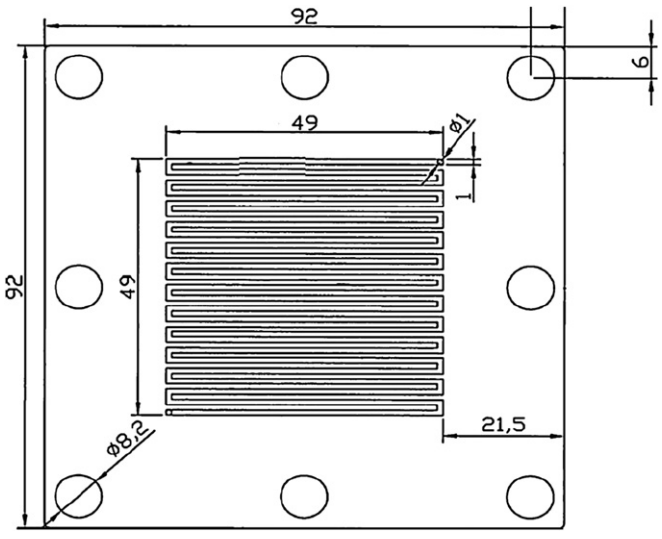

Fig. 2. The schematic diagram of Al-alloy bipolar plate with flow-field pattern.

texturing the surface morphology [22]. In order to increase the contact area of the BPP with GDL and simplify the process, this study used the raw Al-alloy substrate without mechanically polish.

Fig. 3 shows the surface morphology of the Ni–P deposits prepared at 85 °C and various pH values (pH 4.5, 5.5, and 6.5). The morphology of machined marks can still be observed after depositing a thin Ni–P coating on the Al-alloy substrate. Moreover, the pH value is one of the most important factors for surface morphologies and compositions of electroless Ni–P coatings. In the beginning of electroless Ni–P depositing process, Ni^{2+} in the solution reacts first with OH^- to form a transition product, $Ni(OH)_2$, based on the coordination relation. Then, the $Ni(OH)_2$ reacts with $H_2PO_2^-$ to form a complex of $NiOH^+$, and finally reduce to Ni metal state and deposit onto the substrate. Hence, the higher the pH values, the faster growth rate of deposits, and the larger granular size of deposits. As seen in the figures, the surface morphologies of the Ni–P deposits reveal obviously that the amounts of cracks and holes increase with increasing pH values in the electroless bath. That is response to higher pH values with higher driving force of metal reduction in the Ni–P deposition process. It can be expected that the coatings with cracks and holes are prone to be attacked by corrosion media.

Table 5 shows the EDS compositional analyses of Ni–P coatings prepared at various pH values. It is found that the P concentration of Ni–P coatings increased with descending pH values in the baths. Fig. 4 shows the X-ray diffraction results of various Ni–P deposits. The diffraction pattern of the NDU-EN-3 coating shows a sharp Ni (111) peak, but the NDU-EN-2 and NDU-EN-1coatings exhibit an extremely broadened base with a Ni (111) peak. It reveals that the NDU-EN-3 coating has a crystallized structure, but the NDU-EN-2 and NDU-EN-1 coatings possess an amorphous-like or a mixed structure composed of an amorphous matrix and some crystalline regions distributed in the matrix. Moreover, the broadened base of the NDU-EN-1 is wider than that of the NDU-EN-2, indicating that the crystallization degree of the Ni–P coatings increase with increasing pH values in the depositing bath. The P content plays an important role in adjusting the structure and property of Ni–P alloys. While P content in the electroless Ni–P alloys is high enough to a supersaturated state, the Ni–P alloys would become microcrystalline or amorphous structure. The same behavior has been observed in other studies on electroless Ni–P deposition [16].

According to the EDS and XRD analyzed results of the Ni–P coatings, the increase in the pH value caused the decrease of P concentration and better crystallization of electroless Ni–P deposits. However, the Ni–P coatings in amorphous state may possess better corrosion resistance than that of crystalline structure.

3.2. Electroless nickel immersion gold plating

Electroless nickel immersion gold (ENIG) consists of an electroless nickel plating covered with a thin layer of immersion gold, which is reduced from the immersion bath. During the ENIG process, Ni in the electroless Ni–P coating dissolved into the immersion bath and release electrons to promote gold reduction and deposit on the Ni–P coating. Gold possesses excellent conductivity and superior chemical stability, which can be employed to protect the BPP's substrate from corrosion and decrease the interfacial contact resistance between BPP and GDL. Furthermore, the presence of Ni–P coating can enhance the adhesion of gold and aluminum substrate and reduce the usage of gold.

Fig. 5 shows the FE-SEM surface morphology of immersion Au deposited on the Ni–P alloys produced at different pH values,

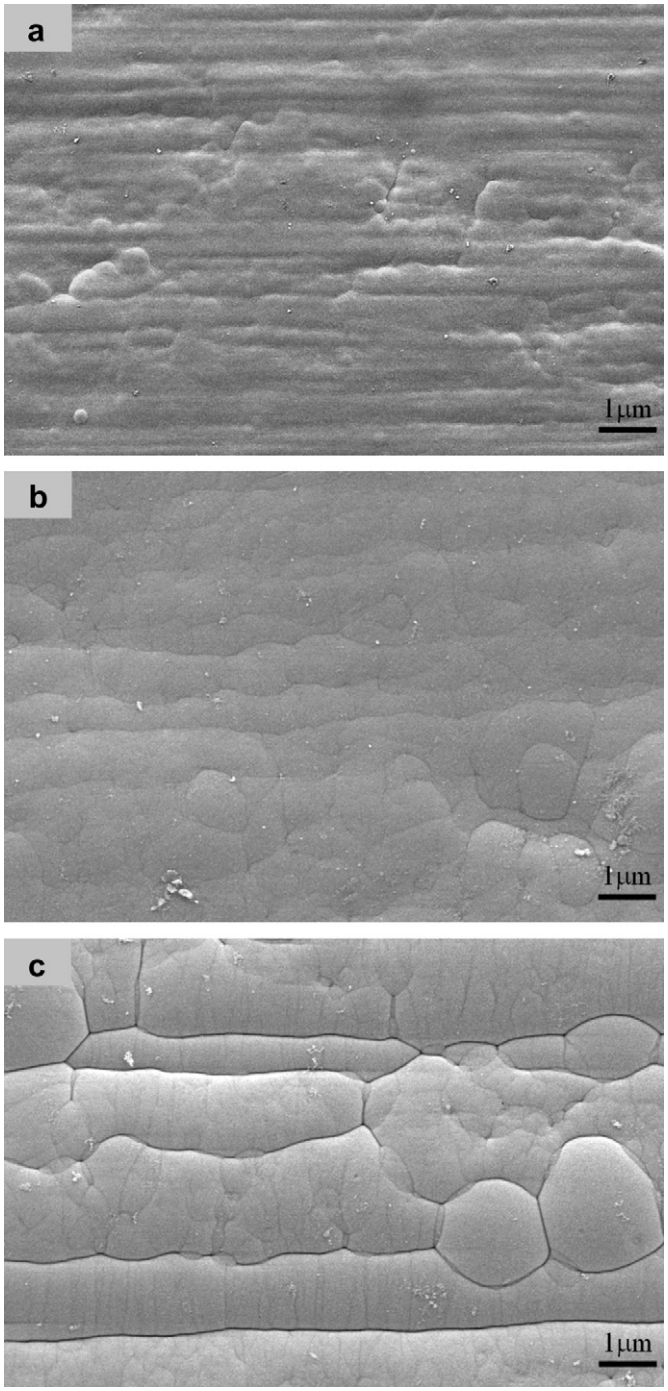

Fig. 3. SEM surface morphologies of the Ni–P deposits prepared at different pH values; (a) NDU-EN-1 (pH 4.5), (b) NDU-EN-2 (pH 5.5), (c) NDU-EN-3 (pH 6.5).

representing that the surface of ENIG plates composed of taper granules. The NDU-ENIG-1 plate surface is fine and smooth. Conversely, the NDU-ENIG-2 and NDU-ENIG-3 plate surface exhibit

Table 5
The composition percentage (at.%) of various Ni–P deposits.

Specimen name	Elements	
	Ni	P
NDU-EN-1 (pH = 4.5)	80.9	19.1
NDU-EN-2 (pH = 5.5)	83.8	16.2
NDU-EN-3 (pH = 6.5)	87.1	12.9

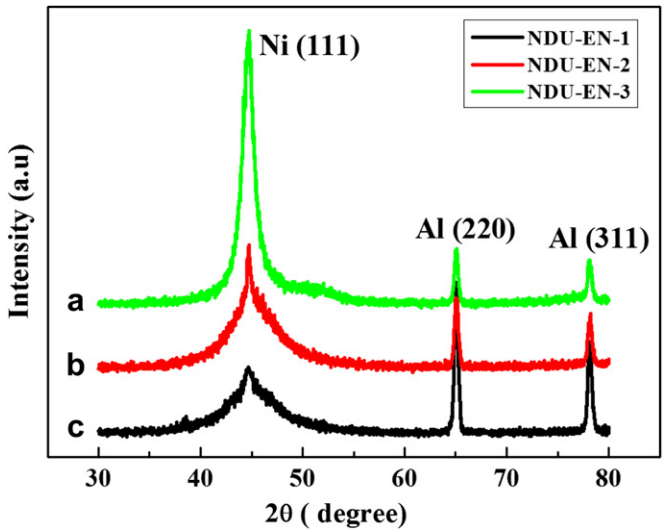

Fig. 4. XRD patterns of Ni–P deposits prepared at various pH; (a) NDU-EN-1, (b) NDU-EN-2, (c) NDU-EN-3.

some crevices and holes. The amounts of crevices and holes on ENIG plates increase with increasing the granular size of Ni–P substrates, indicating that the defects in the ENIG plates increase with increasing the pH values for depositing the Ni–P substrates. Moreover, the defects in the ENIG plates would be the short-cut of corrosion media to attack the substrates.

Fig. 6(a)–(c) presents the cross-sectional SEM images of ENIG deposited on the Ni–P alloys produced at various pH values. All of the Au plates bonded well to the Ni–P alloys, and the Au plate thickness of NDU-ENIG-1, NDU-ENIG-2, and NDU-ENIG-3 is approximately 0.21, 0.37, and 0.52 μm, respectively. It is found that the thickness and structure of the Au plates were obviously changed with the morphology and Ni contents of the Ni–P substrates. As previously mentioned, the Ni–P alloy produced at higher pH value possessed larger granular size, rougher surface morphology, and higher Ni content due to faster deposition rate. Moreover, the electroless Ni–P coating with higher nickel content dissolved larger amounts of Ni to participate in the immersion reaction, and then Au replacement and deposition rate was advanced by large amounts of electrons released from the dissolved nickel. Therefore, the thickness of Au films on the Ni–P substrates is in the order of NDU-ENIG-1 < NDU-ENIG-2 < NDU-ENIG-3. However, the Au film produced on higher Ni-content substrate has more defects (holes) and is looser than that deposited on lower Ni-content substrates, because the Au immersion reaction rate was too fast. Hence, the NDU-ENIG-1 coating is denser and more anti-corrosive than NDU-ENIG-2 and NDU-ENIG-3 coatings.

3.3. Corrosion behaviors of Ni–P and Au/Ni–P coatings

In the previous literature [9], Lin et al. carried out a corrosion test of Ni–P coatings on Al-alloy BPPs in a 0.5 M H_2SO_4 + 2 ppm HF solution, and presented that the nickel-based alloys have excellent protective effect. To compare the corrosion resistance of Ni–P and Au/Ni–P multilayer coatings on the Al-alloy, the corrosion behaviors of the Al-alloy without and with various deposits were investigated via potentiodynamic polarization curve measurements under the same conditions as the previous literature. The polarization curves of all tested specimens are shown in Fig. 7, and corresponding corrosion current density and corrosion potential are listed in Table 6. For the Ni–P coatings, the corrosion current

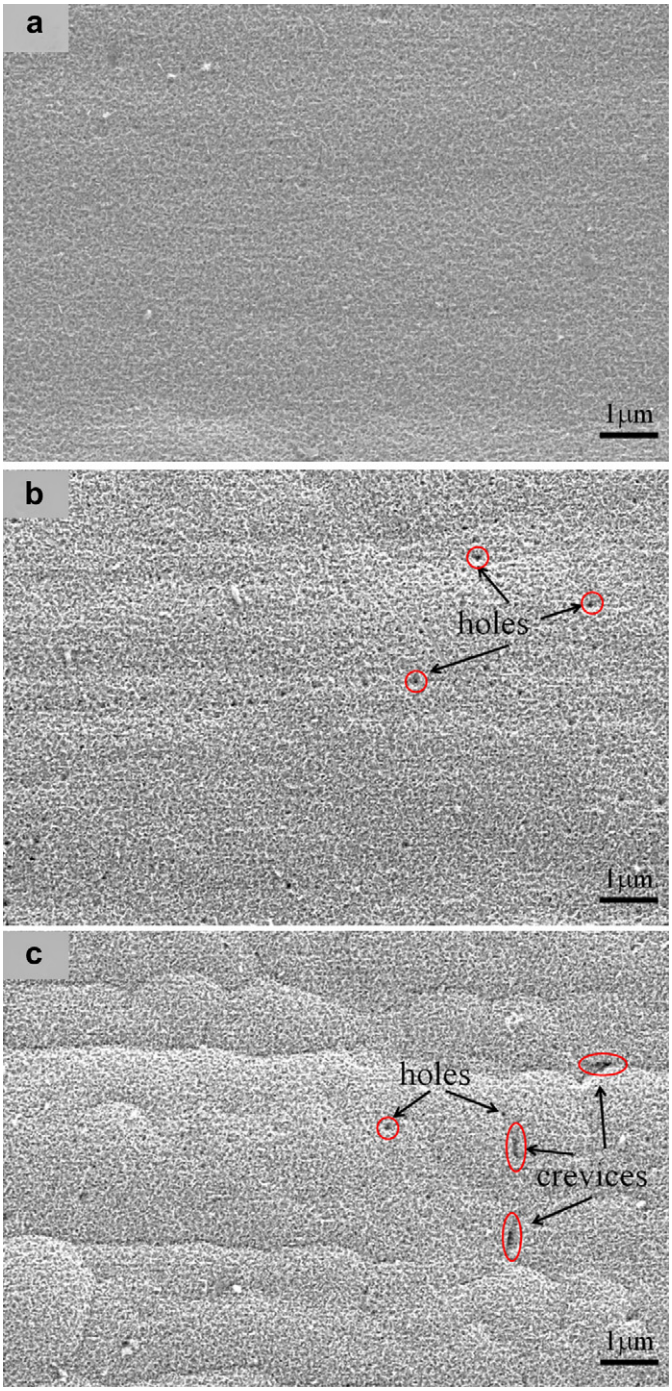

Fig. 5. The surface morphology of electroless nickel immersion gold coatings; (a) NDU-ENIG-1, (b) NDU-ENIG-2, (c) NDU-ENIG-3.

density of NDU-EN-1, NDU-EN-2, and NDU-EN-3 are 8.43×10^{-6}, 1.78×10^{-5}, and 3.41×10^{-5} A cm^{-2}, respectively. This result indicates that the corrosion resistance of NDU-EN-1 coating is better than NDU-EN-2 and NDU-EN-3 coatings. After immersion gold plating process, the corrosion current density of the Al-alloy with NDU-ENIG-1, NDU-ENIG-2, and NDU-ENIG-3 coatings reduced to 3.46×10^{-6}, 9.36×10^{-6}, and 8.64×10^{-6} A cm^{-2}, respectively. From the above results, it is obviously that the corrosion resistance of the Al-alloy is inferior, and both Ni–P and Au/Ni–P multilayer coatings reduce the corrosion rate of the Al-alloy. The corrosion rate of ENIG deposits can be at least 1 or 2 orders of magnitude lower than the Al-alloy.

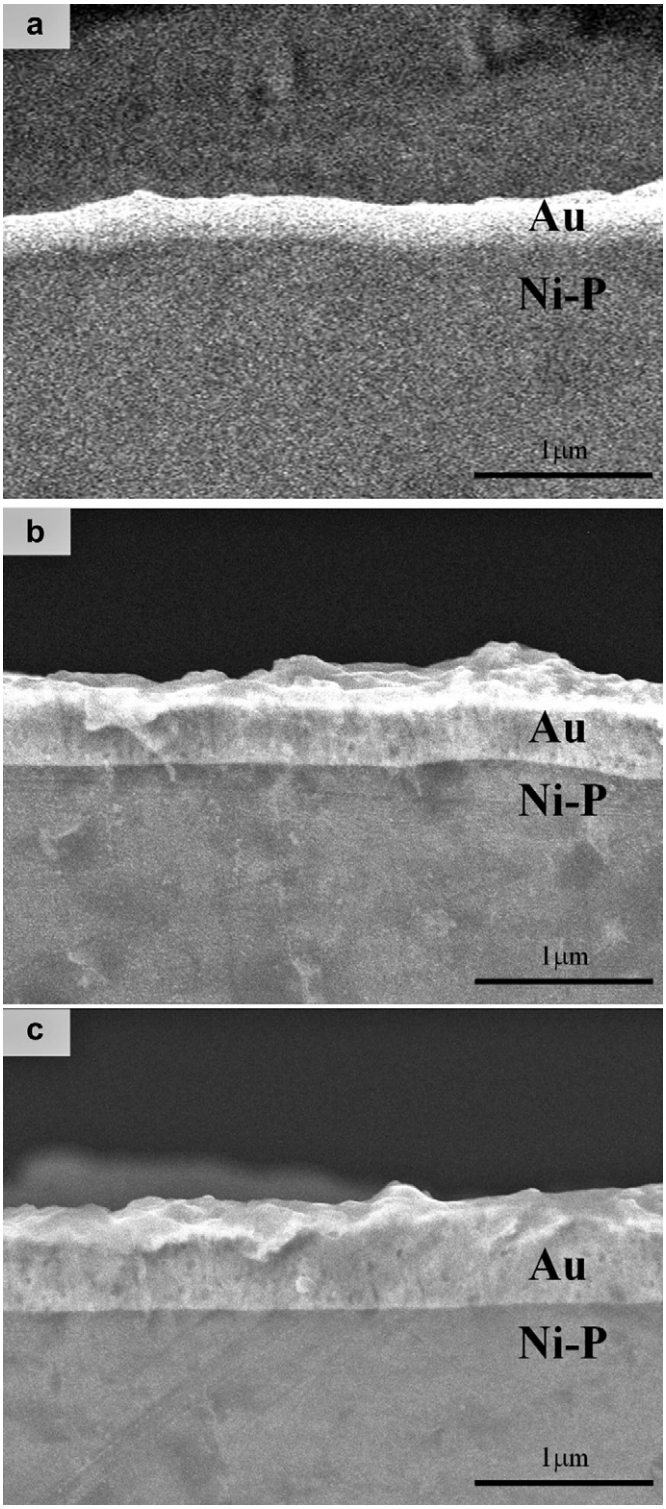

Fig. 6. The cross-sectional images of ENIG coatings; (a) NDU-ENIG-1, (b) NDU-ENIG-2, (c) NDU-ENIG-3.

Comparing the corrosion result of Ni–P with Au/Ni–P coatings, the corrosion potential of ENIG deposits is higher than that of the electroless Ni–P coatings, but the corrosion current density is lower, revealing that the corrosion resistance of the ENIG deposits is better than that of the electroless Ni–P coatings. Moreover, the corrosion resistance of ENIG deposit produced on lower Ni-content substrate (NDU-ENIG-1) is better than that of higher Ni-content substrate (NDU-ENIG-2 and NDU-ENIG-3), because the NDU-ENIG-1 coating is denser than others. This result is in agreement with the SEM observation of the Au/Ni–P coating structures. According to the corrosion test results, the NDU-EN-1 and NDU-ENIG-1 coatings were selected to modify the Al-alloy bipolar plates in a single cell test.

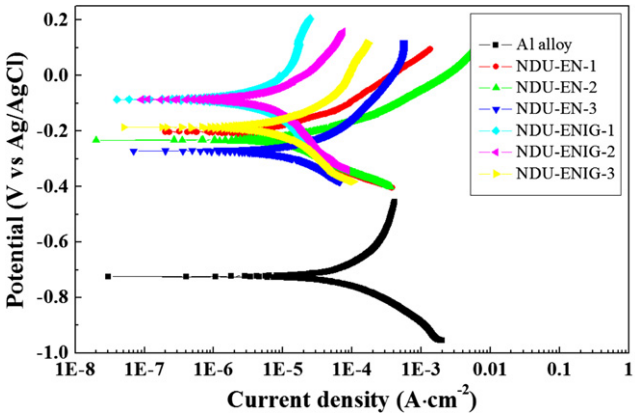

Fig. 7. The polarization curves of the Al-alloy without and with various deposits.

3.4. Interfacial contact resistance

The specimens of bare Al-alloy and that with NDU-EN-1 or NDU-ENIG-1 coatings were employed as the bipolar plates for interfacial contact resistance measurement in this work. Fig. 8 shows the interfacial contact resistance curves of the BPPs (Al-alloy, NDU-EN-1, and NDU-ENIG-1) measured at various compaction pressures. The contact resistance of all measured specimens decrease markedly with increasing compaction pressure as the pressure is lower than 50 N cm^{-2}. At the pressure range of 50–100 N cm^{-2}, the contact resistance decrease moderately with increasing compaction pressure. While compaction pressure is higher than 100 N cm^{-2}, the change of contact resistance is more smooth with raising compaction pressure.

The contact resistance of raw Al-alloy is the highest at various compaction pressures among all tested specimens because of the formation of passive Al oxides on the surface. It is well known that the composition of coating is one of the main factors to affect the ICRs. The specimens with NDU-EN-1 coatings possess lower contact resistance values than that of raw Al alloys, because the Ni–P alloys have the better conductivity than that of Al oxides. In addition, the bipolar plate with NDU-ENIG-1 deposits represent the lowest ICR values, which contribute to high conductivity of Au coating and good bonding between Au and Ni–P alloys. Furthermore, the ICR value of NDU-ENIG-1 is 4 mΩ cm^2 at the compaction pressure of 140 N cm^{-2}, which achieves the goal of U.S. DOE for bipolar plate application. It reveals that the Al-alloy BPP with NDU-

Table 6
The corrosion parameters of the Al-alloy without and with various coatings.

Specimens	I_{corr} (A cm^{-2})	E_{corr} (V)
Al-alloy	1.44×10^{-4}	−0.724
NDU-EN-1	8.43×10^{-6}	−0.194
NDU-EN-2	1.78×10^{-5}	−0.223
NDU-EN-3	3.41×10^{-5}	−0.276
NDU-ENIG-1	2.46×10^{-6}	−0.087
NDU-ENIG-2	9.36×10^{-6}	−0.107
NDU-ENIG-3	8.64×10^{-6}	−0.208

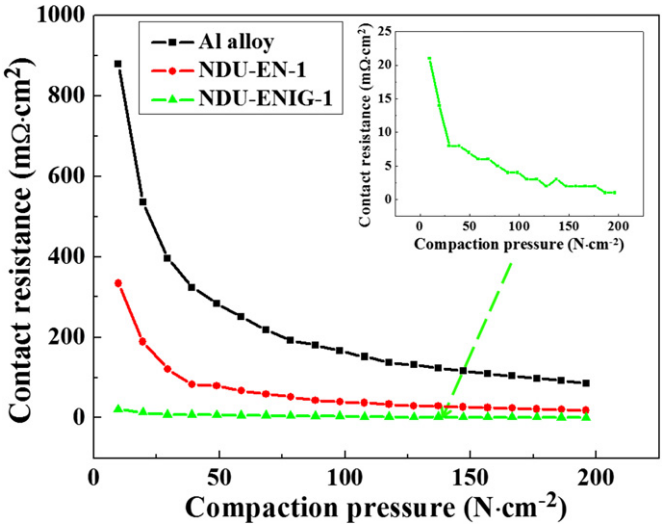

Fig. 8. Interfacial contact resistance of the Al-alloy, NDU-EN-1, and NDU-ENIG-1 as a function of compaction pressures.

ENIG-1 coating has an advantageous effect on surface conductivity for the application in PEM fuel cell systems.

3.5. EIS measurements of single cells

In order to evaluate the decay factors of cell performance, initial and long-term EIS measurements of single cells assembled with the BPPs of graphite, NDU-ENIG-1, NDU-EN-1, and Al-alloy were conducted in the testing environment of 0.6 V and 333 K. Fig. 9(a) and (b) represents the Nyquist plots of the electrochemical impedance spectra at initial and long-term states, respectively, in each cycle consisted of one semicircle in high frequency range. The high frequency impedance of graphite, NDU-ENIG-1, NDU-EN-1, and Al-alloy at initial stage was 7.2, 8.3, 10.5, and 13 mΩ, respectively, indicating that there is a good electrical conductivity (low impedance) between the BPPs and GDLs. The high frequency impedance of graphite and NDU-ENIG-1 increased slightly after 100 h operating, and was 7.7 and 9.1 mΩ, respectively. However, the impedance of NDU-EN-1 and Al-alloy enhanced significantly to 18.6 and 35.9 mΩ, respectively, after only 60 h operating. The result shows the bipolar plates of NDU-EN-1 and Al-alloy were corroded in the cell environment and produced an oxide layer on the surface resulting in an obvious increase of the contact resistance after long-term operating. But, the corrosion resistance of NDU-ENIG-1 BPP is outstanding, and the oxidation is not easy to occur on its surface even undergoing a long-term test.

3.6. Single cell performance

The initial *I–V* curves of single cells assembled with the BPPs of graphite, NDU-ENIG-1, NDU-EN-1, and Al-alloy are compared in Fig. 10. The open circuit voltage (OCV) of the cells fabricated with graphite, NDU-ENIG-1, NDU-EN-1, and Al-alloy is 0.921, 0.923, 0.893, and 0.872 V, respectively. The voltage and performance for the single cell with various BPPs used in this test were similar at low current density, but the difference in the cell performance was becoming large more and more while the operating current density was increasing. It is obviously that the voltage and performance for the single cell with NDU-EN-1 BPPs are higher than those with raw Al-alloy BPPs, but lower than that with NDU-ENIG-1 and graphite BPPs. The voltage and performance of single cell with NDU-ENIG-1 bipolar plates are almost

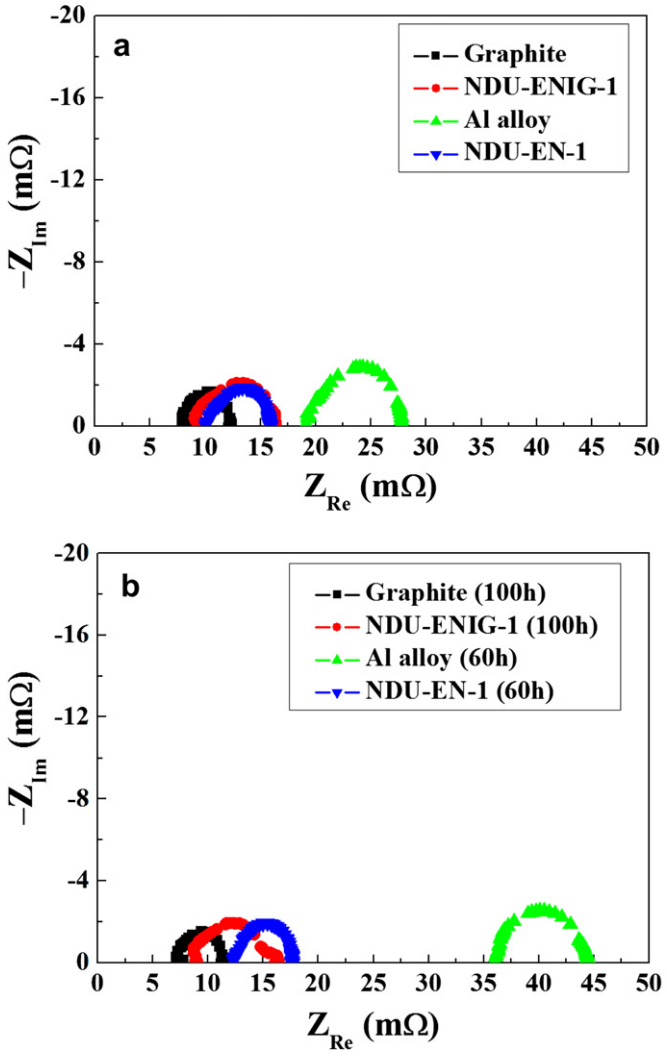

Fig. 9. The Nyquist plots of graphite, NDU-ENIG-1, NDU-EN-1, and Al-alloy bipolar plates constructed at (a) initial and (b) long-term stages.

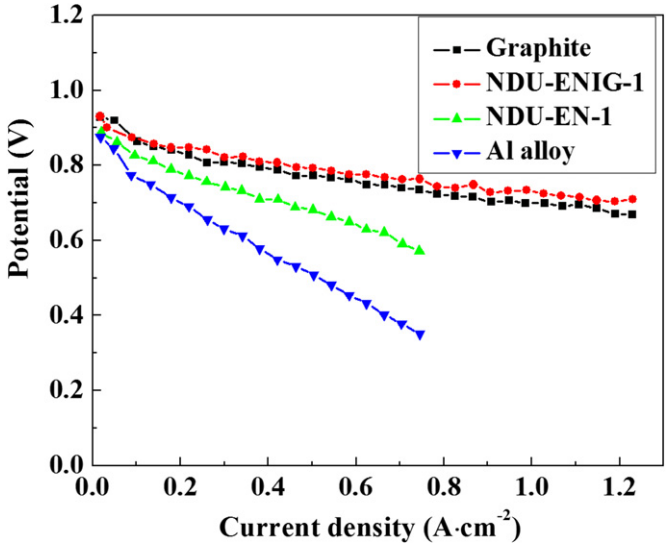

Fig. 10. *I–V* curves of the single cells assembled with graphite, NDU-ENIG-1, NDU-EN-1, and Al-alloy BPPs.

equivalent to that with graphite BPPs at all current density. Moreover, the power density of the cells fabricated with NDU-ENIG-1 BPPs and graphite BPPs is 0.84 W cm^{-2} and 0.80 W cm^{-2} at a cell voltage of 0.7 V, respectively, indicating that the performance of single cell assembled with NDU-ENIG-1 BPPs is better than traditional graphite BPPs. Therefore, the Au/Ni–P multilayer coating exhibits much improved performance and is suitable for the application of Al-based bipolar plates in PEMFC systems.

The BPP's properties that mainly affect the performance of fuel cells are the corrosion resistance and interfacial contact resistance, which are generally related to the superficial composition of coatings. The well performance of NDU-ENIG-1 BPPs can refer to the excellent conductive and anti-corrosive properties of the Au deposit, and the inferior performance of Al-alloy BPPs can attribute to its poor surface conductivity and corrosion resistance. Moreover, the improved performance of Ni–P coatings is not significant for the single cell with NDU-EN-1 BPPs, because the conductive and anti-corrosive properties of Ni–P coatings are insufficient.

4. Conclusions

The Au/Ni–P multilayer coating was produced on Al-based bipolar plates using the electroless nickel immersion gold technique, and its properties and performance for the application to PEMFCs were evaluated. Ni–P coated substrates were prepared at various pH values (pH 4.5, 5.5, and 6.5), and the deposit produced at pH 4.5 (NDU-EN-1) possessed the lowest Ni content (80.9 at.%) and an amorphous state. This deposit has the smoothest surface morphology and the best corrosion resistance among all Ni–P deposits. For preparing Au/Ni–P multilayer coatings, the Au layer deposited on the Ni–P with lowest Ni content (NDU-ENIG-1) is denser and more anti-corrosive in a 0.5 M H_2SO_4 + 2 ppm HF solution than other ENIG coatings.

The bare Al-alloy, NDU-EN-1, and NDU-ENIG-1 bipolar plates were employed for interfacial contact resistance, electrochemical impedance of single cells, and single cell performance measurements. The NDU-ENIG-1 bipolar plate represented the lowest ICR value of 4 mΩ cm^2 at the compaction pressure of 140 N cm^{-2}, which achieves the goal of U.S. DOE for bipolar plate application, because of high conductivity of Au coating and good bonding between Au and Ni–P alloys. The high frequency impedance of NDU-ENIG-1 measured at initial and 100 h operating stages was 8.3 and 9.1 mΩ, respectively, indicating that the oxidation is not easy to occur on NDU-ENIG-1 surface even undergoing a long-term test. The single cell with NDU-ENIG-1 BPPs exhibited a power density of 0.84 W cm^{-2} at a cell voltage of 0.7 V, which is better than that of the cell with traditional graphite BPPs (0.80 W cm^{-2}). Based on the excellent performance presented above, the Al-alloy BPP with NDU-ENIG-1 coating has an advantageous effect on surface conductivity and corrosion resistance for the application in PEM fuel cell systems.

References

[1] I. Bar-On, R. Kirchain, R. Roth, Journal of Power Sources 109 (2002) 71–75.
[2] H. Tsuchiya, O. Kobayashi, International Journal of Hydrogen Energy 29 (2004) 985–990.
[3] D.P. Davies, P.L. Adcock, M. Turpin, S.J. Rowen, Journal of Applied Electrochemistry 30 (2000) 101–105.
[4] J. Larminie, A. Dicks, Fuel Cell Systems Explained, Wiley, New York, 2001.
[5] J. Wind, R. Spah, W. Kaiser, G. Bohm, Journal of Power Sources 105 (2002) 256–260.
[6 A. Hermann, T. Chaudhuri, P. Spagnol, International Journal of Hydrogen Energy 30 (2005) 1297–1302.
[7] H. Tawfik, Y. Hung, D. Mahajan, Journal of Power Sources 163 (2007) 755–767.
[8] R.A. Antunes, M.C.L. Oliveira, G. Ett, V. Ett, International Journal of Hydrogen Energy 35 (2010) 3632–3647.
[9] J.Y. Lin, C.Y. Lin, S.K. Liu, C.C. Wan, Y.Y. Wang, Surface & Coatings Technology 205 (2010) 2251–2255.
[10] C.Y. Bai, Y.H. Chou, C.L. Chao, S.J. Lee, M.D. Ger, Journal of Power Sources 183 (2008) 174–181.
[11] A. Kumar, M. Ricketts, S. Hirano, Journal of Power Sources 195 (2010) 1401–1407.
[12] C. Hartnig, T.J. Schmidt, Electrochimica Acta 56 (2011) 4237–4242.
[13] S.H. Wang, J. Peng, W.B. Lui, J.S. Zhang, Journal of Power Sources 162 (2006) 486–491.
[14] H.Y. Jung, S.Y. Huang, P. Ganesan, B.N. Popov, Journal of Power Sources 194 (2009) 972–975.
[15] W. Qin, Journal of Coatings Technology and Research 8 (2011) 135–139.
[16] X. Haowen, Z. Bangwei, Journal of Materials Processing Technology 124 (2002) 8–13.
[17] A. Bai, P.Y. Chuang, C.C. Hu, Materials Chemistry and Physics 82 (2003) 93–100.
[18] H. Liu, N. Li, S. Bi, D. Li, Journal of The Electrochemical Society 154 (2007) D662–D668.
[19] Y.S. Won, S.S. Park, J. Lee, J.Y. Kim, S.J. Lee, Applied Surface Science 257 (2010) 56–61.
[20] T.M. Wen, K.H. Hou, C.Y. Bai, M.D. Ger, P.H. Chien, S.J. Lee, Corrosion Science 52 (2010) 3599–3608.
[21] H. Wang, M.A. Sweikart, J.A. Turner, Journal of Power Sources 115 (2003) 243–251.
[22] Y. Zhou, G. Lin, A.J. Shih, S.J. Hu, Journal of Power Sources 163 (2007) 777–783.
[23] X. Yuan, H. Wang, J.C. Sun, J. Zhang, International Journal of Hydrogen Energy 32 (2007) 4365–4380.